International Journal of Technology 11(1) 60-70 (2020)
Received May 2019 / Revised July 2019 / Accepted October 2019

International Journal of Technology

http://ijtech.eng.ui.ac.id

The Effect of Ni on the Formation of Bainite in Fe-Ni Lateritic Steels through Semi-continuous Cooling Method

Fatayalkadri Citrawati[1*], Robby Dwiwandono[2], Leksono Firmansyah[2]

[1]*Research Center for Metallurgy and Materials, Indonesian Institute of Sciences, Kawasan PUSPIPTEK, Tangerang Selatan, 15314, Indonesia*
[2]*Sultan Ageng Tirtayasa University, Jl. Jenderal Sudirman KM 3, Cilegon, 42435, Indonesia*

Abstract. The formation of bainite in steel alloys is affected not only by temperature, holding time, and cooling method but also by steel alloy's main alloying element. In iron-nickel (Fe-Ni) lateritic steels, the steelmaking process from nickel pig iron (NPI) gives various Ni contents. In this study, five Fe-Ni alloys with various Ni contents were subjected to semi-continuous austempering. The holding temperatures were 535°C (T1) and 360°C (T2). All alloys were held for 1800 s. Both holding temperatures were determined through the average temperatures of bainite start (Bs) and martensite start (Ms) of each alloy. Observations of the microstructures using an optical microscope and Scanning Electron Microscope (SEM) showed the formation of one or more phases in the alloys. These phases are ferrite as the matrix, degenerated pearlite (DP), lamellar pearlite (LP), and plate-like bainite. In Fe-Ni alloys with Ni content of 0.01 to 2.2 wt% Ni, after holding at either T1 and T2, a mixture of DP and LP in the ferrite matrix is more pronounced. Some plate-like bainite is gradually formed in the 3.3% Ni alloy after holding at T1 and T2. As the Ni content increases to as much as 4.5 wt% Ni, pearlite is no longer visible and is replaced by plate-like bainite in the ferrite matrix. These results indicate that the variation of Ni in Fe-Ni alloys with Ni content less than and equal to 4.5 wt% results in different shapes of bainite, which then affects the mechanical properties of the alloy.

Keywords: Austempering; Bainite; Continuous cooling; Microstructure; Nickel laterite

1. Introduction

The bainite phase in steel alloys is considered a favorable phase for several industrial applications due to its properties and its relatively low-cost production (Wang et al., 2016). In the automotive industry, bainite is understood to absorb energy well during crash trials (Tisza and Czinege, 2018). Meanwhile, in the railway industry, bainite is preferred due to its combination of good weldability (Hlavaty et al., 2009), fatigue resistance, and wear resistance (Vuorinen et al., 2016).

Currently, most developed bainitic steels use manganese (Mn) or chromium (Cr) as their main alloying element (Gong et al., 2015; Hofer et al., 2015; Meng et al., 2015; Toji et al., 2016; Zhou et al., 2017) with added silicon (Si), and almost none use nickel (Ni) as the main alloying element. This may be due to the relatively expensive cost of Ni. However, the lateritic steel alloys produced by the conversion process of nickel pig iron (NPI) from

*Corresponding author's email: fata002@lipi.go.id, Tel.: +62-21-7560911; fax: +62-21-7560553
doi: 10.14716/ijtech.v11i1.3178

lateritic ores need a very minor to no addition of Ni during their steel-making process. Similar to Mn, as an alloying element, Ni is an austenite stabilizer. The addition of Ni provides several benefits, improving corrosion resistance in acidic environments (Cheng et al., 2017), enhancing mechanical properties (Far et al., 2019), and increasing resistance to hydrogen embrittlement (Shim et al., 2017). A steel alloy produced by processing NPI with Ni content less than 4 wt% will have approximately 3 wt% of Ni in the final steel product (Jamali et al., 2014), which is considered a significant amount of Ni in the alloy.

To obtain bainite in a steel alloy, the thermal treatment process includes an isothermal holding by quenching the sample in a salt bath after austenization. However, this method is rarely adopted by the industry (Takayama et al., 2018). In this study, a semi-continuous cooling method is used during thermal treatment. Instead of using a salt bath during the holding process at the bainite transformation temperature, air cooling and a furnace are used to hold the sample at the targeted temperature. It is expected that bainite will form uniformly throughout the sample.

Very few studies consider Fe-Ni steel as bainitic steel. Besides adding economic value to lateritic ore through its Fe-Ni lateritic steel, this study aims to observe further the effect of Ni as a main alloying element with a maximum content of 4.5 wt% on the formation of bainite at two different holding temperatures. These temperatures are considered to be in the temperature range of either lower bainite or upper bainite formation after semi-continuous cooling treatment.

2. Methods

2.1. Materials

The chemical composition of Fe-Ni lateritic alloys used in this study can be found in Table 1.

Table 1 Chemical composition of Fe-Ni lateritic alloys

Code	Chemical Composition (wt%)							
	C	Si	Al	Cr	Ni	P	S	Fe
A	0.3	1.2	0.8	0.02	0.01	<0.01	<0.01	Bal.
B	0.3	1.4	0.7	0.03	1.1	<0.01	<0.01	Bal.
C	0.3	1.4	0.7	0.05	2.2	<0.01	<0.01	Bal.
D	0.3	1.4	1.0	0.05	3.2	<0.01	<0.01	Bal.
E	0.3	1.4	1.0	0.08	4.5	<0.01	<0.01	Bal.

The steel alloys were made using a casting process in a 100 kg induction furnace. The cast plates were then cut to 2 cm × 2 cm × 1 cm to make samples for the study using PresiCut FTC-70MS. The samples were then subjected to thermal treatment, followed by microstructural observations and mechanical testing.

2.2. Heat Treatment

The heat treatment performed in this study is an austempering process to form bainite in the samples. The sequence of the heat treatment process is schematically shown in Figure 1.

The austenization temperature used was 945°C, and the sample was held for 600s at this temperature. During the austempering process, all samples were air cooled to reach the targeted temperatures (T1 and T2) and held for 1800s before the sample was finally air cooled to room temperature outside the furnace chamber. The average cooling rate from the austenization temperature to the targeted austempering temperature is ~13°C/s. This

was calculated using temperature data of the sample obtained using a type K thermocouple and Fluke 54 II data logger.

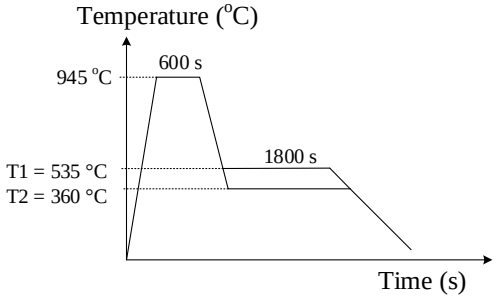

Figure 1 A schematic diagram of the austempering process

The determination of T1 and T2 for all samples was derived from the average calculations of the bainite start temperature (Bs) and martensite start temperature (Ms) of each alloy, which were simulated using JMatPro software. T1 and T2 were then calculated using equations as follows:

$$T1 = \overline{\sum_i Bs_i} \quad (1)$$

$$T2 = \overline{\sum_i Ms_i} \quad (2)$$

where T1 and T2 are the targeted austempering temperatures, Bs_i and Ms_i are the bainite formation temperature and martensite formation temperature of each alloy, respectively, and *i* indexes the alloys, which were alloys A, B, C, D, and E. The simulation was also used to form continuous cooling transformation (CCT) diagrams for each alloy. The measurement parameters were the austenization temperature, which was 945°C, the grain size of 7.3 American Society for Testing and Materials (ASTM), and the chemical composition of each alloy, as listed in Table 1.

2.3. Characterization

Prior to microstructural observations, all thermally treated samples underwent several stages of a mechanical preparation process. They were ground with up to 1200 grit with paper grit and then polished up to 1 μm. The microstructure images were acquired using a Meiji optical microscope and a scanning electron microscope (SEM) JEOL JSM 6390 A, equipped with an electron dispersive spectroscopy (EDS) detector. The etching reagent used was 4% picral. In addition to microstructural observations, all samples were tested for Vicker's hardness using a Mitutoyo HM 200.

3. Results and Discussion

3.1. The Effect of Ni on the CCT Diagram of the Alloys

The calculation results from Equations 1 and 2 for the Fe-Ni alloys in Table 1 give 538.92°C for T1 and 353.16°C for T2. These numbers were rounded down and up to the nearest integers for ease of temperature setting in the furnaces, after which T1 became 535°C and T2 became 360°C. These values are in the temperature range for upper bainite formation and lower bainite formation, respectively (Bhadeshia and Honeycombe, 2017).

The calculated CCT diagrams for alloys A to E indicate each alloy's likeliness of forming different phases, which are austenite, ferrite, pearlite, bainite, and martensite. The distribution of these phases in the alloys will depend on the cooling rate, the temperature, and the hold duration. Figures 2a to 2e show the calculated CCT diagrams for alloys A to E with several simulated cooling rates, which are listed in Table 2.

Table 2 Cooling rates code in Fe-Ni CCT diagrams

Code	Cooling Rate (°C/s)
1	100
2	10
3	1
4	0.1

From these CCT diagrams (Figure 2a – Figure 2e), it can be seen that the variation in Ni content in the alloys has a significant effect on the area of the phases formed. Performing similar heat treatments and cooling rates on all alloys will give various distributions of phases in their microstructures.

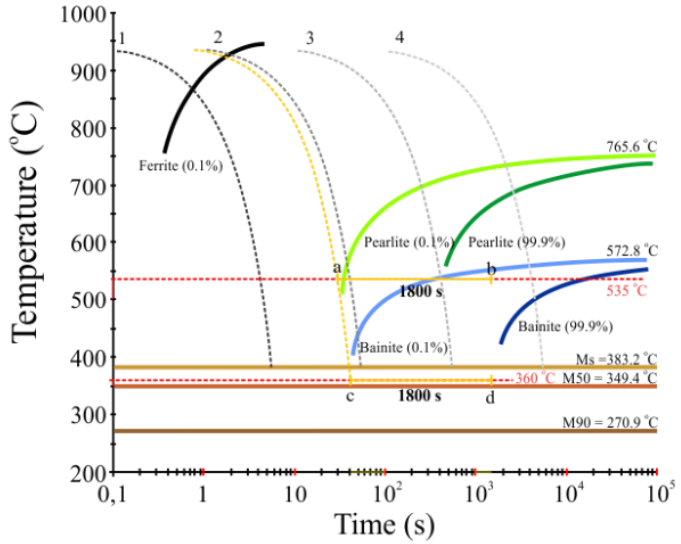

(a)

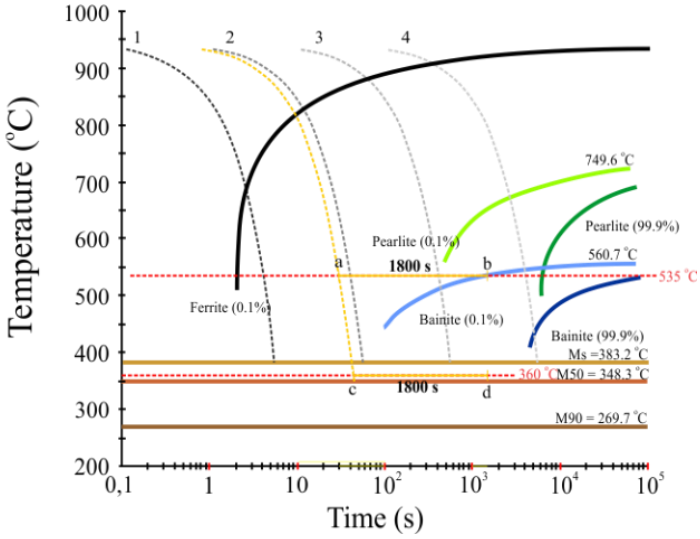

(b)

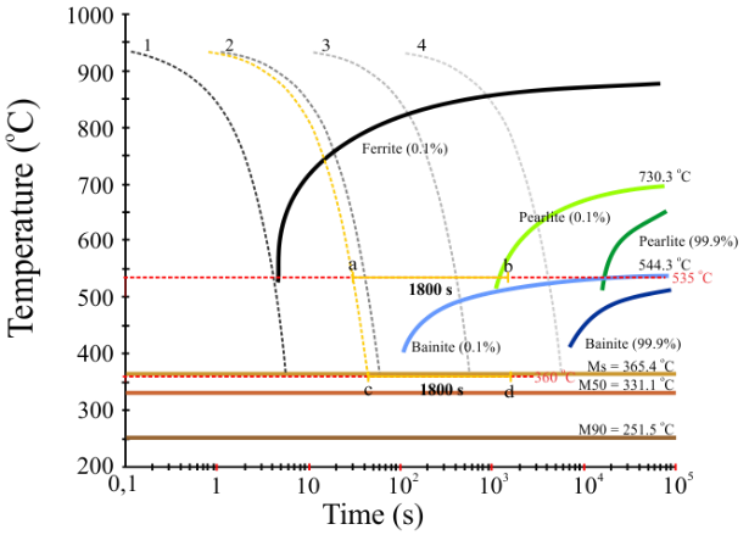

(c)

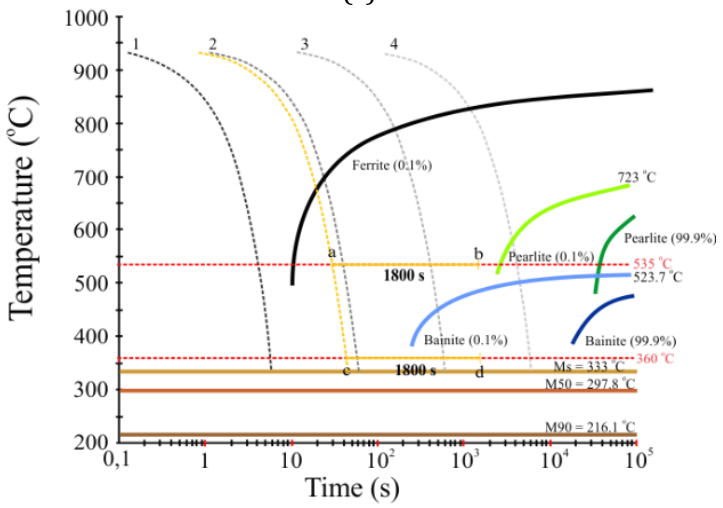

(d)

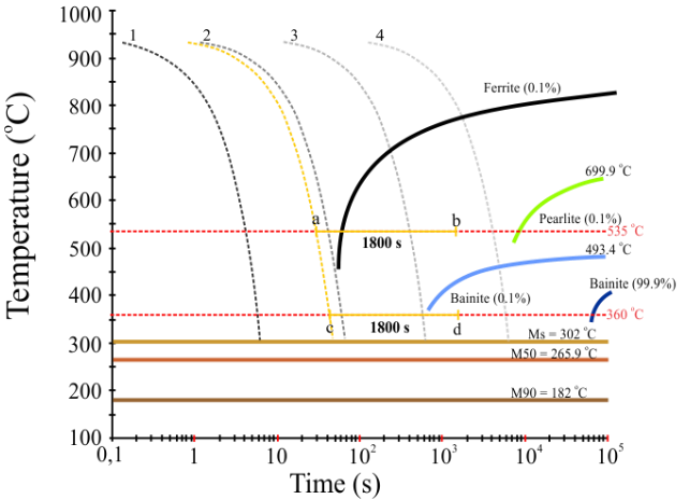

(e)

Figure 2 The calculated CCT diagrams for: (a) alloy A (0.01 wt% Ni); (b) alloy B (1.1 wt% Ni); (c) alloy C (2.2 wt% Ni); (d) alloy D (3.2 wt% Ni); and (e) alloy E (4.5 wt% Ni)

The simulated cooling rates are shown by the dashed gray curves, while the experimental cooling rate is shown by the yellow dashed curve. The holding duration was from points (a) to (b) for temperature T1 and (c) to (d) for temperature T2.

Ferrite, formed previously with cooling rates 1 to 4 in alloy A (Figure 2a), undergoes a significant shift in alloy E (Figure 2e). The addition of Ni to as much as 4.5 wt% shifts the ferrite area toward a slower cooling rate line. Therefore, in alloy E, ferrite will only be formed if the heat treatment is conducted at cooling rates 3 or 4. The shift of the ferrite area towards these slower cooling rate lines indicates that increasing Ni content enables the enlargement of the area for austenite.

The area shifting also occurred for pearlite and bainite. These two phases differ in their formation temperatures, which allows pearlite to form before bainite. In alloy A, the starting lines for both pearlite and bainite formation are located in the same time range. As the Ni content increases from alloy B to alloy E, the areas for both pearlite and bainite are displaced to slower cooling rate lines.

The addition of Ni affects pearlite more significantly than bainite. As shown in alloys B to E (Figure 2b – Figure 2e), even though both phases experience an area shift, the transformation start line for pearlite is displaced to a much slower time range than for bainite.

For martensite, the addition of Ni in the alloys results in a change in area by shifting its transformation start line to a lower temperature. In alloy A, the Ms is calculated to be 383°C. This temperature falls to 302°C in alloy E. This temperature decrease indicates that bainite is allowed to form at lower temperatures as the Ni content increases.

From the heat treatment scheme performed in this study, a dashed line showing the experimental cooling rate (~13°C/s) is drawn in all calculated CCT diagrams. It is located near line 2. Points (a) and (b) indicate the beginning and the end of the holding duration for T1, respectively, while points (c) and (d) indicate the beginning and the end of the holding duration for T2, respectively.

While holding at T1, the experimental heat treatment lines of all alloys pass across the bainite area at different stages. The lines for alloys A and B pass across the bainite area at the end of their holding processes (Figure 2a – Figure 2b), while for alloys C, D, and E, the lines pass across the bainite area during the air cooling after holding (Figure 2c – Figure 2e).

While holding at T2, it is shown that in alloys A to C, the holding process is predicted to occur below their Ms temperatures (Figure 2a – Figure 2c). This is the opposite of alloys D and E, in which their holding processes are above their Ms temperatures (Figure 2c and Figure 2d). At this holding temperature, even though T2 is quite close to the Ms, the c-d holding lines for alloys D and E are able to pass across the Bs before the final cooling. Therefore, it is expected that bainite is formed in these alloys.

3.2. The Effect of Ni on the Microstructure Developments

Figure 3 shows the final microstructure of the samples after they were subjected to either T1 or T2 of the heat treatment sequences shown in Figure 1, resulting in different phase morphologies, sizes, and distributions. As predicted in the calculated CCT diagrams (Figure 2a – Figure 2e), the cooling process from the austenization temperature to the austempering temperature, either T1 or T2, followed by air cooling, will allow ferrite (light area) to form in all alloys.

The effect of Ni added to the alloys is indicated by the morphology and distribution of the cementite-containing phase (dark area) in samples prepared at both T1 and T2. The cementite-containing phase can be pearlite, bainite, or even martensite. However, it is difficult to differentiate these phases at optical-level resolution. The grain size of the cementite-containing phase varies depending on the austempering temperature and the amount of Ni added to the alloy. The grain shape of the cementite-containing phase in alloys

A to C appears as blocky areas in various sizes, whereas in alloys D and E this previously blocky area becomes needle-like in shape and is distributed evenly throughout the area.

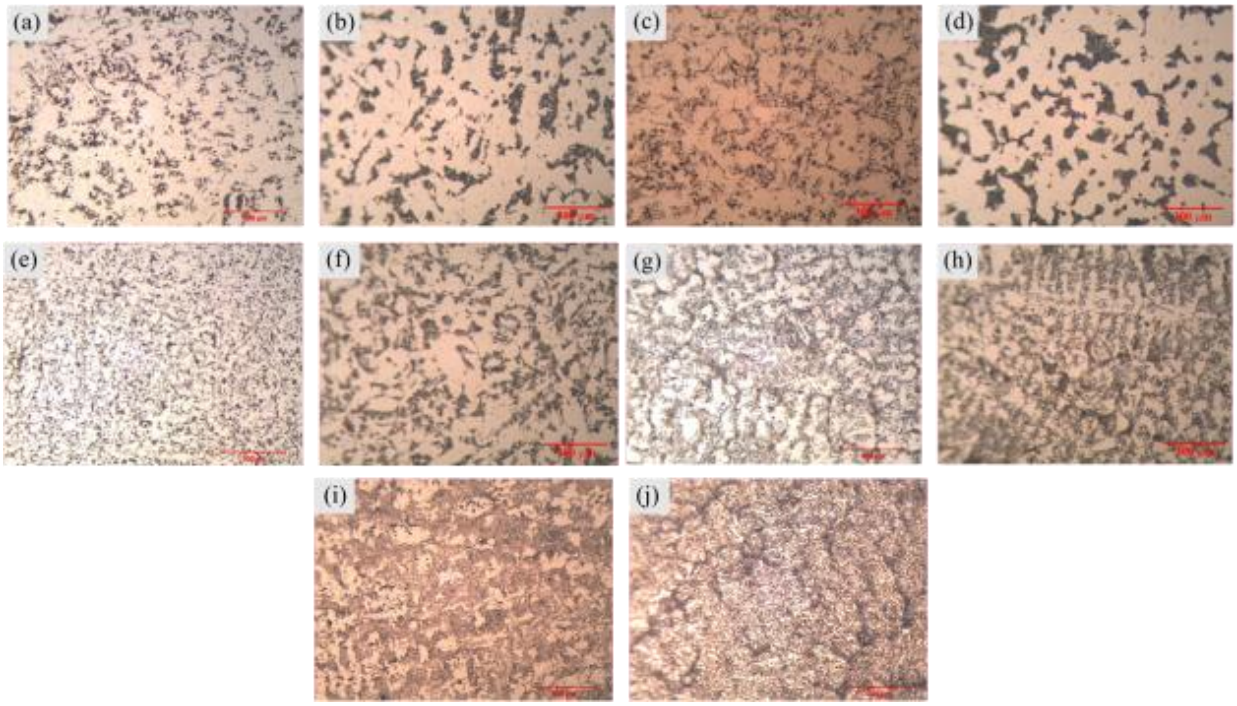

Figure 3 Microstructure images of: (a) sample T1 alloy A; (b) sample T2 alloy A; (c) sample T1 alloy B; (d) sample T2 alloy B; (e) sample T1 alloy C; (f) sample T2 alloy C; (g) sample T1 alloy D; (h) sample T2 alloy D; (i) sample T1 alloy E; and (j) sample T2 alloy E. The dark areas are cementite-containing phases, while the light areas are the ferrite matrix

As depicted in Figures 3a and 3b, for alloy A, sample T1 shows much finer dark blocky areas than sample T2. From the average grain size graph in Figure 4, sample T1 of alloy A has an average grain size of ~26.4 μm, while the dark blocky area in sample T2 of alloy A has an average grain size of ~102.8 μm.

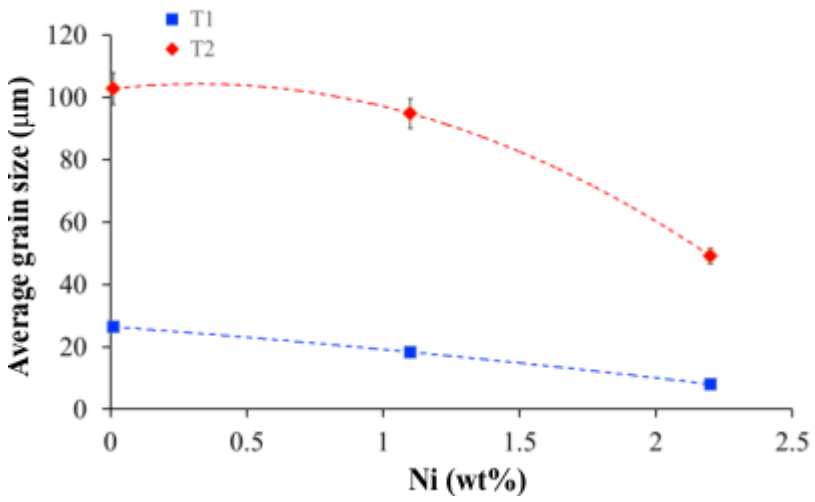

Figure 4 The average grain size of the cementite-containing phase in alloys A to C after austempering at T1 and T2

In alloy B, both sample T1 (Figure 3c) and sample T2 (Figure 3d) show no significant difference in their dark blocky areas compared to alloy A. However, as Figure 4 shows, the

average grain sizes of the cementite-containing phase in samples T1 and T2 of alloy B are lower than for samples T1 and T2 of alloy A. For alloy B, the average grain size is ~18.4 μm and ~94.8 μm for samples T1 and T2, respectively.

In alloy C, with Ni content increased to 2.2 wt%, the dark areas start changing their shape. In Figure 3e, sample T1 of alloy C has much smaller grains than the grains in sample T1 of alloy B. These dark areas in alloy C are evenly distributed in the ferrite matrix. In sample T2 of alloy C, Figure 3f, the dark blocky area starts to split into smaller dark areas separated by the ferrite matrix, which is similar to sample T1 of alloys A and B (Figures 3a and 3c). In alloy C, the average grain size of the cementite-containing phase is ~8 μm for sample T1 and ~49.2 μm for sample T2.

As Figure 4 shows, overall, as the Ni content increases from 0.01 to 2.2 wt%, the T2 samples experience a more significant decrease in average grain size in the cementite-containing phase compared to the T1 samples, which is as much as 53.6 μm for T2 samples compared to only 18.4 μm for T1 samples.

The evenly distributed granular shape of the dark area in its ferrite matrix in sample T1 of alloy C becomes a group of needle-like shapes in sample T1 of alloy D (Figure 3g). The needle-like shapes have an average grain size of ~4.87 μm and are distributed as small groups throughout the ferrite matrix. Similar to sample T1 of alloy D, sample T2 of alloy D (Figure 3h) also has a different microstructure from sample T2 of alloy C (Figure 3f). In sample T2 of alloy D, the cementite-containing phase is more evenly distributed compared to sample T2 of alloy C. The dark area has needle-like shapes with an average size of ~1.84 μm.

In alloy E, with Ni content of 4.5 wt%, both sample T1 (Figure 3i) and sample T2 (Figure 3j) have an arrangement of needle-like shapes in the cementite-containing phase. However, in sample T1 of alloy E, among the groups of needle-like dark areas, several blocky areas of ferrite still appear. In contrast, in sample T2 of alloy E, the needle-like phase is more evenly distributed in the matrix.

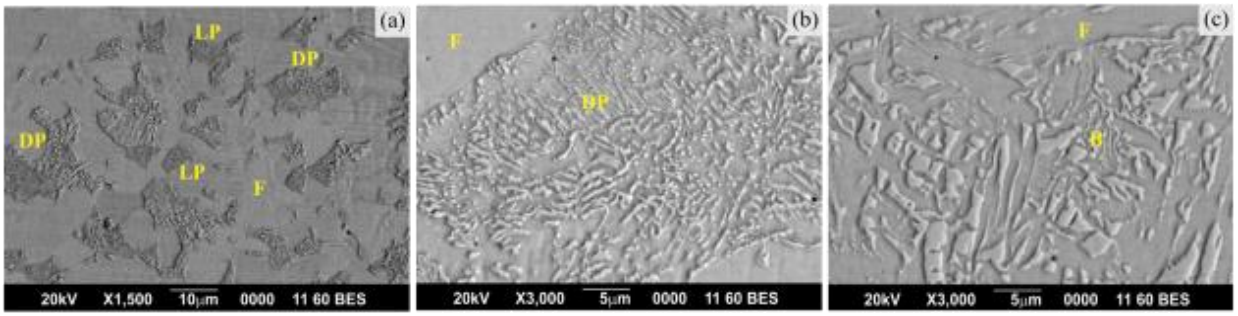

Figure 5 SEM images of: (a) sample T1 alloy B; (b) sample T2 alloy B; and (c) sample T2 alloy E. DP is degenerated pearlite, LP is lamellar pearlite, F is ferrite, and B is bainite

The dark areas of all the samples were then observed further using SEM. The SEM images of the samples show some distribution differences in the cementite-containing phase. In Figure 5a, for sample T1 of alloys A, B, and C, the dark areas mostly have a lamellar shape or layers like pearlite. Besides this lamellar pearlite (LP), there is an area with a combination of lamellar and granular shapes with the lamellar distance wider than LP, which is called degenerated pearlite (DP).

DP, also known as granular bainite (Furuhara et al., 2007), is usually formed in a eutectoid or hypoeutectoid steel alloy. It has a finer cementite size (Kim et al., 2013) and forms at lower temperatures than LP. Since the samples undergo a semi-continuous cooling process, it is likely that during holding at either T1 or T2, the temperature is still gradually

decreasing to reach either T1 or T2. Therefore, both LP and DP might be able to form in one sample.

For sample T2, Figure 5b shows that the dark area seen in the microstructure of sample T2 of alloys A, B, and C is a DP grain. The difference between samples T1 and T2 in both alloys A and B is that sample T1 has more LP than DP, whereas sample T2 has more DP than LP. Even though the T2 samples of alloys A, B, and C were subjected to a holding temperature below Ms, martensite is not found in their microstructures. Martensite is formed without carbon diffusion, while the formation of pearlite, either LP or DP, involves carbon diffusion (Embury, 2012) at different rates and temperatures.

In Figure 5c, a significant morphological difference between the dark area of alloys A, B, and C and alloys D and E occurred in both samples T1 and T2.

In samples T1 and T2 of alloy D, some LP still exists compared to sample T1 of alloy C. In these samples, plate-like bainite has started to form, even though its grain size is not as big as shown in Figure 5c. For alloy E, pearlite is no longer visible in either sample T1 or T2. In its place, blocky areas and plates of bainite are seen in both samples.

3.3. The Effect of Ni on the Hardness Distributions

The graph in Figure 6a shows the correlation between hardness and Ni content for all T1 and T2 samples. For alloy A, the hardness of the T1 and T2 samples is almost the same, with sample T1 slightly higher than sample T2. The value of hardness is increased for samples with higher Ni content (from 1.1 to 4.5 wt% Ni) after they were subjected to the same heat treatment sequence, either at T1 or T2. Furthermore, samples which were subjected to holding at temperature T2 are shown to have a slight increase in hardness compared to samples subjected to holding at temperature T1, especially for alloys B to E.

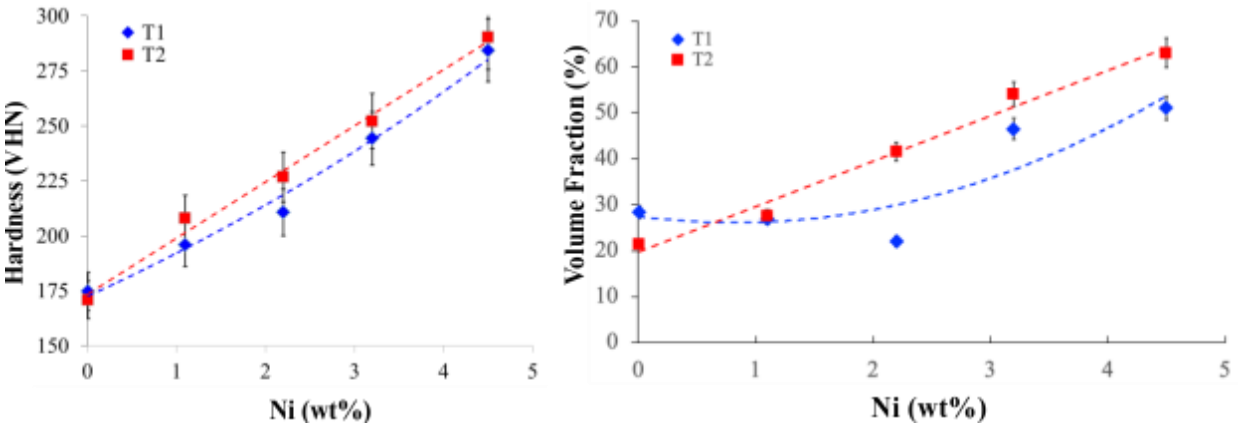

(a) (b)

Figure 6 (a) The hardness value of all samples after the austempering process at T1 and T2. (b) The average volume fraction of the dark areas (cementite-containing phase) in all samples after austempering at T1 and T2

The increase in hardness for most T2 samples might be caused by a difference in the volume fraction of the cementite-containing phase in samples T1 and T2 for alloys B to E. Figure 6b shows the correlation between the average volume fractions of the dark areas in each alloy with their Ni contents. As shown in the Figure 6b graph, the T1 samples for alloys B to E have a slightly lower average volume fraction of the dark area than the corresponding T2 samples. This indicates that less area of cementite carbide will result in lower hardness.

Moreover, the hardness of sample T2 of alloys A to C confirms that martensite is not formed during the holding process since the hardness range of these alloys is in ~175 to ~225 Vicker's Hardness Number (VHN).

4. Conclusions

The semi-continuous cooling heat treatment process with holding temperatures at T1 and T2 produced bainite in all samples, along with a ferrite matrix and pearlite with various morphologies and distributions.

The microstructures of samples held at 535°C (T1) and 360°C (T2) were observed to contain gradually less pearlite as the Ni content increased. In the alloy containing the highest concentration of Ni (4.5 wt% in alloy E), pearlite was not visible. Instead, the microstructure found in this alloy was plate-like bainite with blocky areas of ferrite as the matrix.

Subjecting samples to the lower holding temperature resulted in larger average sizes of the dark areas (cementite-containing phase) and higher volume fractions of dark areas and, thus, higher hardness. However, as the Ni content increases, holding at either 535°C or 360°C semi-continuously results in a smaller grain size of the dark areas. This decrease in the average grain size of dark areas was more pronounced in samples held at 535°C or at temperatures closer to Bs. In contrast, the hardness and the volume fraction of the cementite-containing phase increased as the Ni content increased.

With the same treatment parameters, the variation of Ni in Fe-Ni alloys in the range of 0.01 to 4.5 wt% affects the morphology of bainite formed in the as-treated samples, which then affects their mechanical properties.

Acknowledgments

This study was funded by the Competence Research Program 2017–2019 under the Research Group for National Steel Based on Laterite at the Research Center for Metallurgy and Materials – Indonesian Institute of Sciences (P2MM LIPI).

References

Bhadeshia, H., Honeycombe, R., 2017. *Steels: Microstructure and Properties*. 4th Edition. Chapter 6, Butterworth-Heinemann, Massachussets, USA, pp. 179–202

Cheng, X., Jin, Z., Liu, M., Li, X., 2017. Optimizing the Nickel Content in Weathering Steels to Enhance Their Corrosion Resistance in Acidic Atmospheres. *Corrosion Science*, Volume 115, pp. 135–142

Embury, D., 2012. The Formation of Pearlite in Steels. *In:* Phase Transformation in Steels: Fundamentals and Diffusion Controlled Transformations. Volume 1. Pereloma, E. & Edmonds, D.V. (ed.), Woodhead Publishing in Materials, Cambridge, UK, pp. 276–310

Far, A.R.H., Anijdan, S.H.M., Abbasi, S.M., 2019. The Effect of Increasing Cu and Ni on a Significant Enhancement of Mechanical Properties of High Strength Low Alloy, Low Carbon Steels of HSLA-100 Type. *Materials Science and Engineering: A*, Volume 746, pp. 384–393

Furuhara, T., Moritani, T., Sakamoto, K., Maki, T., 2007. Substructure and Crystallography of Degenerate Pearlite in an Fe-C Binary Alloy. *Materials Science Forum*, Volume 539–543, pp. 4832–4837

Gong, W., Tomota, Y., Harjo, S., Su, Y.H., Aizawa, K., 2015. Effect of Prior Martensite on Bainite Transformation in Nanobainite Steel. *Acta Materialia*, Volume 85, pp. 243–249

Hlavaty, I., Sigmund, M., Krejci, L., Mohya, P., 2009. The Bainitic Steels for Rails Applications. *Materials Engineering*, Volume 16(4), pp. 44–50

Hofer, C., Leitner, H., Winkelhofer, F., Clemens, H., Primig, S., 2015. Structural Characterization of "Carbide-free" Bainite in a Fe–0.2C–1.5Si–2.5Mn Steel. *Materials Characterization*, Volume 102, pp. 85–91

Jamali, A., Binudi, R., Adjiantoro, B., 2014. *Proses Dekarburisasi Nickel Pig Iron* (Decarburising Process of Nickel Pig Iron). *Metalurgi*, Volume 29(2), pp. 153–160

Kim, H., Kang, M., Jung, H.J., Kim, H.S., Bae, C.M., Lee, S., 2013. Mechanisms of Toughness Improvement in Charpy Impact and Fracture Toughness Tests of Non-heat-treating Cold-drawn Steel Bar. *Materials Science and Engineering: A*, Volume 571, pp. 38–48

Meng, J., Feng, Y., Zhou, Q., Zhao, L., Zhang, F., Qian, L., 2015. Effects of Austempering Temperature on Strength, Ductility and Toughness of Low-C High-Al/Si Carbide-Free Bainitic Steel. *Journal of Materials Engineering and Performance*, Volume 24(8), pp. 3068–3076

Shim, D.H., Lee, T., Lee, J., Lee, H.J., Yoo, J.-Y., Lee, C.S., 2017. Increased Resistance to Hydrogen Embrittlement in High-strength Steels Composed of Granular Bainite. *Materials Science and Engineering: A*, Volume 700, pp. 473–480

Takayama, N., Miyamoto, G., Furuhara, T., 2018. Chemistry and Three-dimensional Morphology of Martensite-austenite Constituent in the Bainite Structure of Low-carbon Low-alloy Steels. *Acta Materialia*, Volume 145, pp. 154–164

Tisza, M., Czinege, I., 2018. Comparative Study of the Application of Steels and Aluminum in Lightweight Production of Automotive Parts. *International Journal of Lightweight Materials and Manufacture*, Volume 1(4), pp. 229–238

Toji, Y., Matsuda, H., Raabe, D., 2016. Effect of Si on the Acceleration of Bainite Transformation by Pre-existing Martensite. *Acta Materialia*, Volume 116, pp. 250–262

Vuorinen, E., Ojala, N., Heino, V., Rau, C., Gahm, C., 2016. Erosive and Abrasive Wear Performance of Carbide Free Bainitic Steels – Comparison of Field and Laboratory Experiments. *Tribology International*, Volume 98, pp. 108–115

Wang, K., Tan, Z., Gao, G., Gao, B., Gui, X., Misra, R.D., Bai, B., 2016. Microstructure-property Relationship in Bainitic Steel: The Effect of Austempering. *Materials Science and Engineering: A*, Volume 675, pp. 120–127

Zhou, M., Xu, G., Tian, J., Hu, H., Yuan, Q., 2017. Bainitic Transformation and Properties of Low Carbon Carbide-Free Bainitic Steels with Cr Addition. *Metals*, Volume 7(7), pp. 263–275